





## Article

# Use of CdS from Teaching-Laboratory Wastes as a Photocatalyst for the Degradation of Fluoroquinolone Antibiotics in Water

Efraím A. Serna-Galvis <sup>1,2</sup>, Yenny Ávila-Torres <sup>3,\*</sup> , María Ibáñez <sup>4</sup> , Félix Hernández <sup>4</sup>   
and Ricardo A. Torres-Palma <sup>2,\*</sup> 

- <sup>1</sup> Grupo de Investigaciones Biomédicas Uniremington, Facultad de Ciencias de la Salud, Corporación Universitaria Remington (Uniremington), Calle 51 No. 51-27, Medellín 050010, Colombia; efrain.serna@uniremington.edu.co
- <sup>2</sup> Grupo de Investigación en Remediación Ambiental y Biocatálisis (GIRAB), Instituto de Química, Facultad de Ciencias Exactas y Naturales, Universidad de Antioquia UdeA, Calle 70 No. 52-21, Medellín 050010, Colombia
- <sup>3</sup> Grupo de Investigación QUIBIO, Facultad de Ciencias Básicas, Universidad Santiago de Cali, Calle 5 No. 62-00, Pampalinda, Santiago de Cali 760035, Colombia
- <sup>4</sup> Environmental and Public Health Analytical Chemistry, Research Institute for Pesticides and Water (IUPA), University Jaume I (UJI), Avda. Sos Baynat, S/N, 12071 Castellón, Spain; ibanezm@uji.es (M.I.); hernandf@uji.es (F.H.)
- \* Correspondence: yennytorres@usc.edu.co (Y.Á.-T.); ricardo.torres@udea.edu.co (R.A.T.-P.)



**Citation:** Serna-Galvis, E.A.; Ávila-Torres, Y.; Ibáñez, M.; Hernández, F.; Torres-Palma, R.A. Use of CdS from Teaching-Laboratory Wastes as a Photocatalyst for the Degradation of Fluoroquinolone Antibiotics in Water. *Water* **2021**, *13*, 2154. <https://doi.org/10.3390/w13162154>

Academic Editors: Sergi Garcia-Segura and José Alberto Herrera-Melián

Received: 2 June 2021

Accepted: 19 July 2021

Published: 5 August 2021

**Publisher's Note:** MDPI stays neutral with regard to jurisdictional claims in published maps and institutional affiliations.



**Copyright:** © 2021 by the authors. Licensee MDPI, Basel, Switzerland. This article is an open access article distributed under the terms and conditions of the Creative Commons Attribution (CC BY) license (<https://creativecommons.org/licenses/by/4.0/>).

**Abstract:** Laboratory wastes containing Cd<sup>2+</sup> and water polluted by pharmaceuticals represent an environmental concern. In this work, a proof concept, consisting of the use of teaching-laboratory wastes to synthesize CdS and its subsequent use as a photocatalyst to degrade fluoroquinolone antibiotics, was developed. The CdS was prepared by extraction with thioacetamide and calcination (at 450 °C) and characterized using several techniques. The photocatalytic activity of the CdS, to degrade levofloxacin and norfloxacin, was tested, and the routes involved in the process and the primary transformations of the fluoroquinolones were established. Moreover, the ability of CdS-photocatalysis to eliminate levofloxacin in simulated matrices of fresh urine and hospital wastewater was evaluated. The characterization analyses indicated that the CdS semiconductor was synthesized successfully. Effectively, the CdS acted as a photocatalyst toward degradation of levofloxacin, involving the action of superoxide anion radical, holes, and singlet oxygen mainly. The process induced transformations on the methyl-piperazyl moiety, plus hydroxylation of the fluoroquinolone nucleus on levofloxacin. Additionally, CdS-photocatalysis was highly selective for the elimination of the target pollutant in both tested matrices. Our research indicated the good potentiality of recycling teaching-laboratory wastes to generate photocatalysts to degrade organic pollutants. This work was presented at 4<sup>o</sup> Congreso Colombiano de Procesos Avanzados de Oxidación (4CCPAOx).

**Keywords:** advanced oxidation process; catalyst synthesis; levofloxacin; norfloxacin; pollutants removal; wastes reuse; water treatment

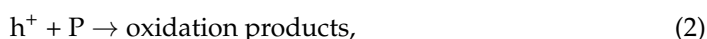
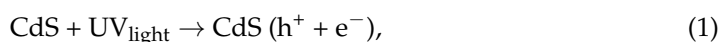
## 1. Introduction

The circular economy has appeared as a possible solution to make better use of resources and to minimize environmental pollution. This is an actual trend, which proposes the reuse and/or the generation of value-added products from wastes [1]. The present research was performed under the circular economy concept. Herein, a proof of concept for the recycling of teaching-laboratory wastes as reagents to prepare a photocatalyst, and its subsequent use to degrade organic pollutants in aqueous matrices, is presented. It is important to mention that in the teaching laboratories of universities a variety of wastes are generated, which must be collected and responsibly discarded, to minimize their impact on the environment and human health [2]. Since the 1980s of the last century, aqueous solutions containing metals such as cadmium are considered hazardous wastes, even if the

metal concentrations are low [3]. In this sense, wastewater containing cadmium represent a serious risk for both the environment and humans.

In both aquatic and terrestrial ecosystems, cadmium tends to bioaccumulate, particularly in vertebrates, specifically in their kidneys and liver. Moreover, algae and plants can accumulate cadmium [4]. When cadmium is ingested by humans, it decreases bone density and disrupts bone composition. The growth of bones is very sensitive to cadmium effects, so children have high risks. Furthermore, cadmium is not easily excreted and tends to accumulate, thereby inducing kidney diseases [5]. Considering the environmental issues of cadmium, its release from laboratory wastes must be avoided. Metal ions such as  $\text{Cd}^{2+}$  can be precipitated as hydroxides or sulfides; however, after minimizing the volume, the problem of final waste disposal may remain [3]. Thus, the resultant solids from precipitation should be reused in other processes.

In this context, the present research shows a proof of concept for the synthesis of CdS from teaching-laboratory wastes and its use as a photocatalyst for the elimination of organic pollutants in water matrices. It is important to mention that CdS is a semiconductor, whose interaction with UV light promotes the generation of an electron–hole pair (Equation (1)) [6,7]. The photo-generated hole has oxidizing properties and can directly degrade organic pollutants (P) (Equation (2)). Meanwhile, the electron in the conduction band reacts with dissolved oxygen in water, forming superoxide anion radical ( $\text{O}_2^{\bullet-}$ , Equation (3)) [8]. In turn,  $\text{O}_2^{\bullet-}$  may evolve toward hydrogen peroxide (Equation (4)) and hydroxyl radical ( $\text{HO}^\bullet$ , Equation (5)). Reactive oxygen species such as  $\text{O}_2^{\bullet-}$ ,  $\text{H}_2\text{O}_2$ , and  $\text{HO}^\bullet$  degrade organic contaminants (Equation (6)) [9–12]. It should be indicated that the redox potential ( $E^\circ$ ) for the  $\text{h}^+$  in CdS corresponds to  $\sim 1.7$  V [13], which is lower than required to oxidize water ( $E^\circ = 2.31$  V at pH 7 [14]) or hydroxyl anion ( $E^\circ = 1.9$  V [15]). Then, the direct production of hydroxyl radicals by the action of the hole is limited.



On the contrary, pharmaceuticals belong to the so-called contaminants of emerging concern [16]. Specifically, fluoroquinolone antibiotics are used worldwide, showing incomplete removal by conventional wastewater treatment plants. Thereby, these pharmaceuticals are present in different environmental water matrices at hazardous concentrations [17]. This is the case of levofloxacin (LEV) and norfloxacin (NOR), two highly consumed fluoroquinolones, which are frequently found in environmental water and effluents of municipal wastewater treatment plants. These compounds can promote the proliferation of antibiotic-resistant bacteria [16–19]. Consequently, for some bacterial infections, the clinical usefulness of fluoroquinolones is limited [20].

The photocatalytic process could be an alternative to degrade fluoroquinolones such as LEV and NOR. Therefore, this work reports a proof of concept for the synthesis of CdS from teaching-laboratory wastes and its use as a photocatalyst to degrade fluoroquinolone antibiotics. Our research comprised the following stages: (i) To characterize the synthesized CdS obtained from laboratory solution wastes; (ii) to test the photocatalytic activity of CdS toward the degradation of levofloxacin and norfloxacin from water; (iii) to elucidate the degradation routes involved in the photocatalytic and primary transformations of pollutants; and (iv) to evaluate the performance of CdS-photocatalysis in two matrices (synthetic urine and simulated hospital wastewater) more complex than distilled water.

## 2. Materials and Methods

### 2.1. Reagents

LEV was purchased from Sigma-Aldrich (St Louis, MO, USA). NOR was provided by Laproff Laboratories (Medellín, Colombia). Acetonitrile, benzoquinone, furfuryl alcohol, isopropanol, methanol, potassium iodide, sodium acetate, sodium chloride, sodium dihydrogen phosphate, sodium hydroxide, sodium sulfate, sulfuric acid, and urea were provided by Merck (Darmstadt, Germany). Ammonium chloride, calcium chloride, formic acid, and magnesium chloride were provided by PanReac (Barcelona, Spain). Thioacetamide was provided by Sigma-Aldrich (St. Louis, MO, USA).

The solutions were prepared using distilled water. For the determination of the degradation routes involved in the photocatalytic process, scavengers (i.e., isopropanol, benzoquinone, furfuryl alcohol, and potassium iodide) were used at a concentration 100-fold higher than the antibiotic.

For UHPLC–HRMS analysis, HPLC-grade water was obtained by purifying demineralized water using a Milli-Q system from Millipore (Bedford, MA, USA). HPLC-grade methanol and acetonitrile, formic acid, acetone, and sodium hydroxide were acquired from Scharlau (Barcelona, Spain). Leucine enkephalin was purchased from Sigma-Aldrich (St. Louis, MO, USA).

### 2.2. Synthesis of CdS

Cadmium ions were obtained as a liquid waste (which also contained lead (II)) from the experimental practices of inorganic and analytical chemistry courses at a university teaching laboratory. A sample of the liquid waste (50 mL) was mixed with thioacetamide up to complete precipitation of the cadmium ions. The obtained solid was placed in a furnace at 450 °C to remove the organic matter. After this, the synthesized CdS was recrystallized with distilled water at 45 °C.

### 2.3. Reaction Systems for the Fluoroquinolone Degradation

The photocatalytic process was carried out in a homemade aluminum reflective reactor box equipped with five BLB UVA lamps (Philips, Piła, Poland; with the main emission peak at 365 nm, 15 W each; Figure S1 in the Supplementary Materials). The actual intensity of the light inside the reactor was 40 W m<sup>-2</sup>, which was measured using a SOLAR PMA2000 radiometer (SOLAR LIGHT CO, Glenside, PA, USA). Fluoroquinolone solutions (55 mL) were placed in beakers under constant stirring.

### 2.4. Analyses

#### 2.4.1. CdS Characterization

The synthesized CdS was characterized using a high-resolution confocal BX441 spectrometer (OLYMPUS, Tokyo, Japan) equipped with a CCD detector, and a laser excitation source in solid-state for 784.29 nm. Scanning electron microscopy (SEM) images were obtained using a JSM-7800F SEM (JEOL, Tokyo, Japan) (a field emission electron microscope at 5 kV). The study of the chemical composition was carried out through an energy-dispersive X-ray spectroscopy (EDS) system (Apollo XL3 + HiKari) from EDAX PEGASUS (Mahwah, NJ, USA) at 15 kV. X-ray diffraction patterns were carried out in an X'Pert PRO-MRD (PW3050/65) diffractometer from PANalytical in a grazing incident (Malvern, UK) (0.60) using K $\alpha$  Co radiation. The UV-Vis-NIR spectra (diffuse reflectance analysis, 40,000–4000 cm<sup>-1</sup>) were recorded on a Cary-5E (Varian, Palo Alto, CA, USA) spectrophotometer. The modified Kubelka–Munk function allowed the determination of E<sub>gap</sub> [21]. Transmission electron microscopy (TEM) analyses were performed using a TECNAI F20 SUPERTWIN equipment (Model 20-063-15, FEI, Hillsboro, OR, USA). The TEM specimens were prepared following 200 Kv, 97.00 kX–450.00 kX parameters. The Brunauer–Emmett–Teller (BET) surface area, pore size, and pore volume distributions were determined at 350 °C for 240 min, under high vacuum conditions for degassing. The isotherm was carried out in the pressure range of 0.1–0.998 p/p<sup>0</sup>, adsorption, and

desorption (50 points minimum), and it was chosen the region where the curve was not negative. The specific surface area ( $S_{\text{BET}}$ ) was determined by applying the BET equation.

#### 2.4.2. Chromatographic Analyses

The evolution of fluoroquinolones was followed using a UHPLC Dionex UltiMate 3000 instrument (Thermo Fisher Scientific, Bartlesville, OK, USA) equipped with an Acclaim™ 120 RP C18 column (Thermo Fisher Scientific, Bartlesville, OK, USA) (5  $\mu\text{m}$ , 4.6  $\times$  150 mm) and a diode array detector set at the maximum wavelengths of fluoroquinolones (280 and 290 nm for norfloxacin and levofloxacin, respectively). The injection volume was 20  $\mu\text{L}$ . The mobile phase was 10 mmol L<sup>-1</sup> of formic acid (pH 3.0)/acetonitrile at 85/15 (% *v/v*), in isocratic mode (1 mL min<sup>-1</sup>).

Transformation products (TPs) were elucidated by UHPLC–HRMS using a Waters Acquity UPLC system (Waters, Milford, CT, USA), coupled to a hybrid quadrupole-orthogonal acceleration time-of-flight mass spectrometer (XEVO G2 QTOF, Waters Micromass, Manchester, UK), with an orthogonal Z-spray–ESI interface, operated in both positive and negative ionization modes. Additional details on the instrumental conditions can be found elsewhere [22].

#### 2.4.3. Adsorption in Dark, Degradation Rate Determination, and Cd (II) Leaching

The pharmaceuticals were in contact with the CdS in the dark for 15 min to achieve the adsorption/desorption equilibrium (the pollutants adsorption on the catalyst was low (<15%)). Afterward, the UVA light was turned on.

The antibiotics removal was evaluated by determining the initial degradation rate ( $r$ ), which was calculated as the plot slope of concentration vs. time, taking the first points (as illustrated in Figure S2). Therefore, the kinetics are associated with the degradation (with low competence of the transformation products). The experiments were carried out at least by duplicate.

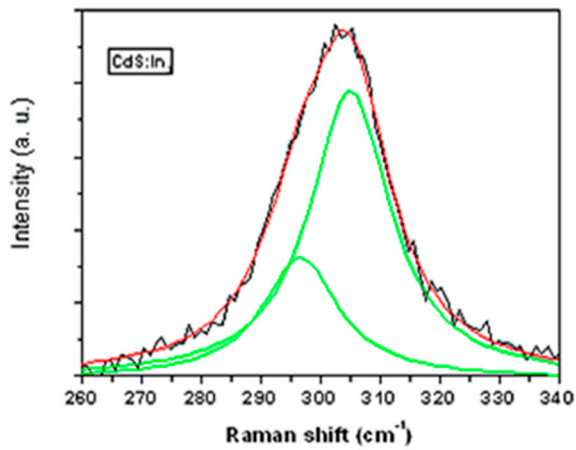
Leaching of cadmium (II) ions from the synthesized CdS was determined by atomic absorption spectrometry according to the method described by Fang et al. [23] using an iCE 3000 Series instrument (Thermo Fisher Scientific, Bartlesville, OK, USA).

### 3. Results

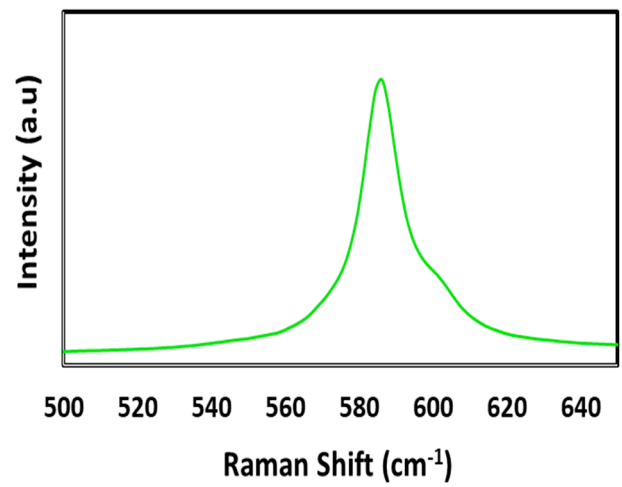
#### 3.1. Characterization of the Synthesized CdS (RAMAN, SEM, EDS, TEM, BET, and Diffuse Reflectance)

RAMAN, EDS, SEM, TEM, BET, and diffuse reflectance analyses were performed for the synthesized CdS. Concerning the RAMAN spectra, the phonon vibrational modes of the prepared material were observed. Moreover, typical signals of CdS at  $\sim 300\text{ cm}^{-1}$  (Figure 1a) and  $\sim 600\text{ cm}^{-1}$  (Figure 1b) were found, while additional signals between 700 and  $1000\text{ cm}^{-1}$  were not observed. The SEM micrograph, at the 1  $\mu\text{m}$  scale (Figure 1c), revealed that the surface morphology of the solid was characterized by large amounts of voids. The surface was not homogenous, and a mixture of hexagonal crystals and distorted cubes was observed. Figure 1d shows the TEM images of CdS (at the 20 nm scale), indicating that this material had an average diameter of 3–5 nm. In the TEM images, the shape of these nanoparticles was in agreement with that observed in the SEM images.

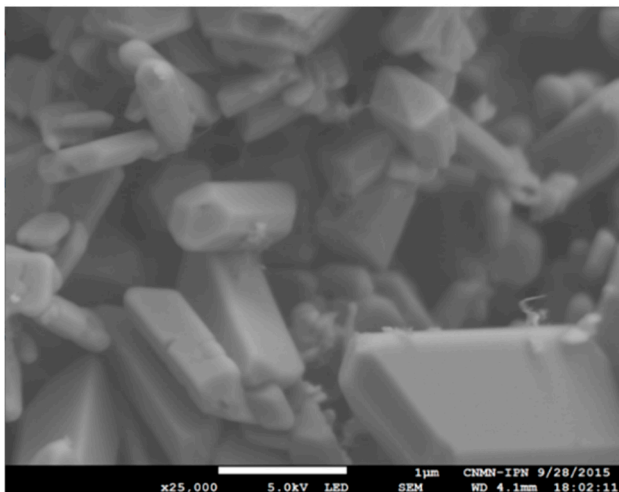
From the EDS analysis, it was determined that the predominant elements in the compound were Cd (49%) and S (49%), and there were lesser amounts of the elements Pb and C ( $\sim 2\%$ ). The diffuse reflectance spectrum showed transitions to lower energy associated with a band-gap ( $E_{\text{gap}}$ : 2.62 eV; Figure 1e). Figure 1f shows the N<sub>2</sub> adsorption–desorption isotherm for CdS, which allowed us to determine the  $S_{\text{BET}}$  (0.2974 m<sup>2</sup> g<sup>-1</sup>) and pore volume (0.0022 cm<sup>3</sup> g<sup>-1</sup>).



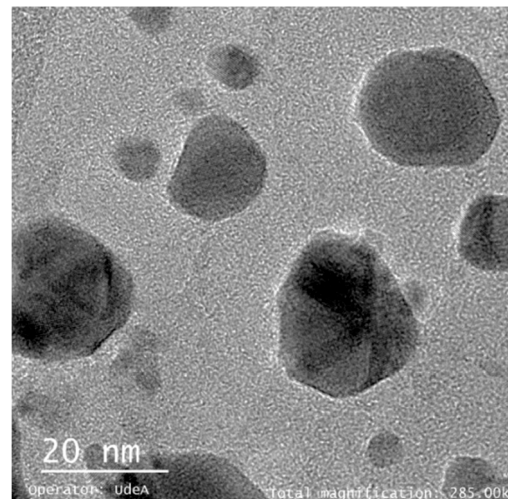
(a)



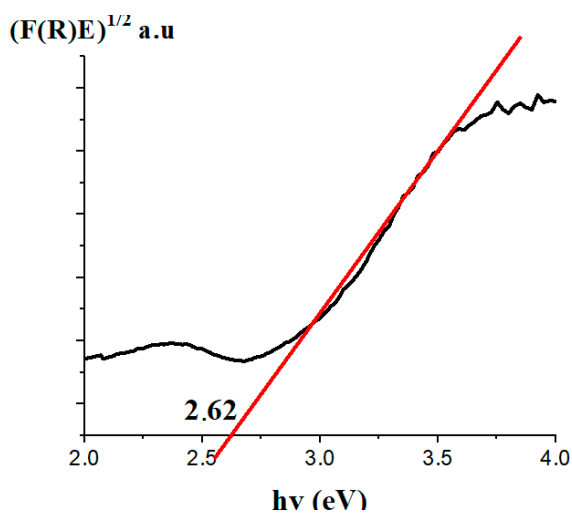
(b)



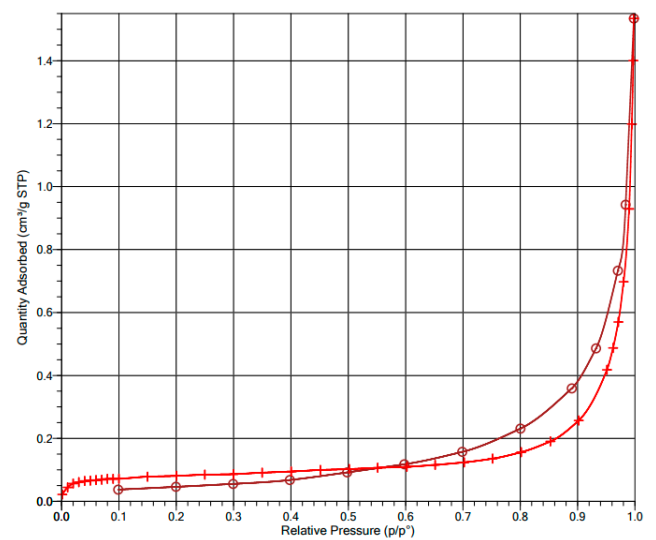
(c)



(d)



(e)



(f)

**Figure 1.** CdS characterization. (a) RAMAN spectrum (260–340  $\text{cm}^{-1}$ ), (b) RAMAN spectra (500–640  $\text{cm}^{-1}$ ), (c) SEM micrograph, (d) TEM image, (e) diffuse reflectance spectrum, and (f) BET adsorption-desorption loop.



### 3.2. Effect of Fluoroquinolone Structure

To obtain information about the effect of fluoroquinolone structure on the photocatalytic process, the degradations of levofloxacin (LEV) and norfloxacin (NOR) were considered. Initially, the action of the UVA light alone on levofloxacin (LEV) was tested and compared to the response of norfloxacin (NOR). After evaluation of the photolysis of the antibiotics promoted by UVA, the photocatalytic treatment (i.e., UVA/CdS) was tested. Figure 2 presents the degradation rate for these fluoroquinolones under UVA alone and the UVA/CdS process. In turn, Figure S3 contains the UV-vis spectra of NOR and LEV.

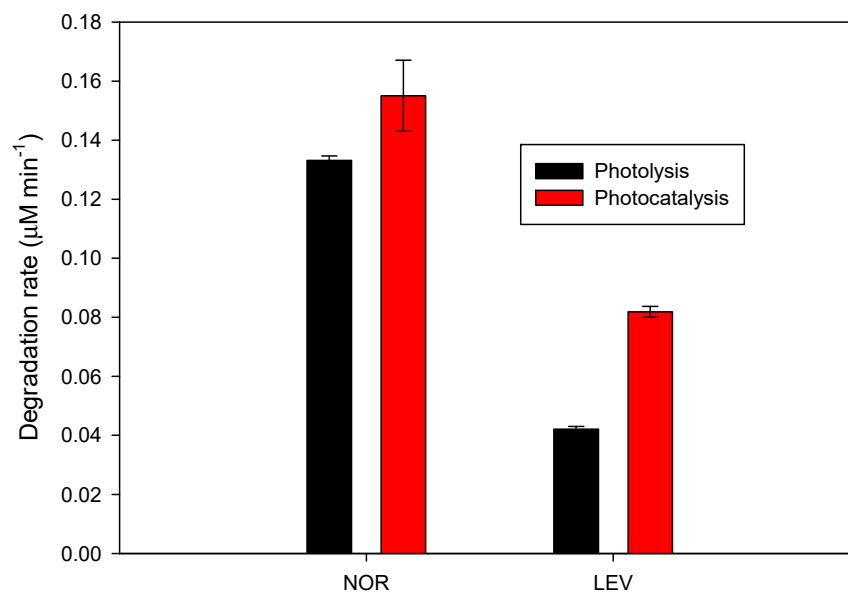


**Figure 2.** Degradation rates for the treatment of NOR and LEV by photolysis (UVA alone) and photocatalysis (UVA/CdS). Experimental conditions: [NOR] = [LEV] = 13.8 µM, [CdS] = 0.5 g L<sup>-1</sup>, UVA intensity = 40 W m<sup>-2</sup>, and initial pH = 5.3.

### 3.3. Effect of Levofloxacin Concentration

In photolysis and photocatalysis with semiconductors, the effect of the pollutant concentration is typically assessed to determine the kinetics involved in the degradation [9]. Thus, in this work, degradation of LEV by UVA and UVA/CdS at different concentrations was performed (Figure S4).

The photolytic process (UVA alone) exhibited a linear response of the degradation rate with an increase in the pollutant concentration, and its kinetics can be expressed by Equation (7), where  $r$  represents the rate of photolytic degradation,  $k$  is a pseudo-first-order constant, and  $C_0$  means the initial concentration of LEV.

$$r = kC_0. \quad (7)$$

On the contrary, it is well-known that the Langmuir–Hinshelwood (L-H) model is the most typical kinetics for heterogeneous photocatalytic processes [24]. Thus, for the UVA/CdS system, the fitting of the experimental data to the L-H model was evaluated. This model is represented by Equation (8), where  $C$  is the initial concentration of the pollutant,  $k_{L-H}$  means the apparent rate constant and  $K_{L-H}$  represents the adsorption–desorption equilibrium constant [9]. To calculate these parameters, Equation (8) can be linearized as shown in Equation (9). Table 1 summarizes the kinetics results for both systems (i.e., photolytic and photocatalytic).

$$r = k_{L-H} K_{L-H} C / (K_{L-H} C + 1), \quad (8)$$

$$C/r = (C/k_{L-H}) + (1/k_{L-H} K_{L-H}). \quad (9)$$

**Table 1.** Kinetics analyses for photolytic and photocatalytic degradation of LEV.

Initial Concentration (Co in $\mu\text{M}$ )	Photolytic System (UVA Alone)		Photocatalytic System (UVA/CdS)	
	$r_{\text{experimental}}$ ( $\mu\text{M min}^{-1}$ )	$r_{\text{adjusted with Equation (7)}}$ ( $\mu\text{M min}^{-1}$ )	$r_{\text{experimental}}$ ( $\mu\text{M min}^{-1}$ )	$r_{\text{adjusted with Equation (8)}}$ ( $\mu\text{M min}^{-1}$ )
4.3	0.0038	0.0044	0.0371	0.0390
13.8	0.0249	0.0236	0.0747	0.0705
23.4	0.0421	0.0427	0.0818	0.0834
<b>Kinetics values</b>	k: $0.002 \text{ min}^{-1}$		$k_{\text{L-H}}$ : $0.112 \mu\text{M min}^{-1}$ ; $K_{\text{L-H}}$ : $0.126 \mu\text{M}^{-1}$	
<b>APE (%) *</b>	7.4		4.2	

\* APE (average percentage error) was calculated as reported by Chiha et al. [25].

### 3.4. Routes of Degradation and Primary Transformations

To determine the participation of reactive species in the photocatalytic degradation of LEV, several experiments in the presence of scavengers were carried out. Isopropanol (IPA), furfuryl alcohol (FFA), potassium iodide (KI), and benzoquinone (BQ) were used to establish the participation of hydroxyl radicals, singlet oxygen, photo-generated holes, and superoxide anion radical, respectively [26–28]. The ratio ( $R_r$ ) between the degradation rate in the presence and absence of each scavenger was determined (Equation (10)). A value of  $R_r$  equal to 1 means that the species has no participation in the degradation, whereas a value of  $R_r$  lower than 1 indicates that the species contributes to the LEV elimination. Figure 3 contains the  $R_r$  values.

$$R_r = \text{rate in scavenger presence} / \text{rate in scavenger absence.} \quad (10)$$

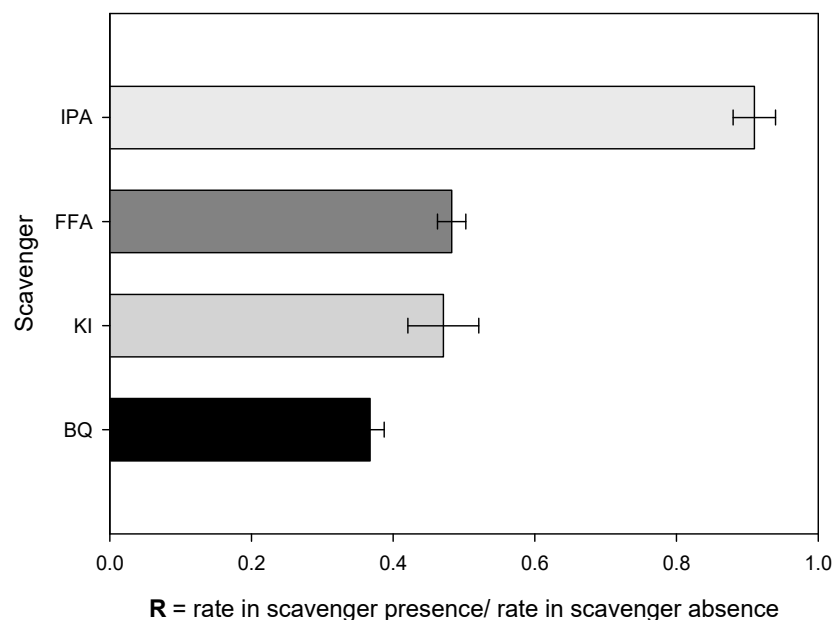


**Figure 3.** Effect of scavengers on the degradation of LEV. Experimental conditions:  $[\text{LEV}] = 13.8 \mu\text{M}$ ,  $[\text{IPA}] = [\text{FFA}] = [\text{KI}] = [\text{BQ}] = 1.38 \text{ mM}$ ,  $[\text{CdS}] = 0.5 \text{ g L}^{-1}$ , UVA intensity =  $40 \text{ W m}^{-2}$ , and initial pH = 5.3.

In contrast, the structural elucidation of primary TPs was carried out by UHPLC–HRMS. Figures S5 and S6 show the MS/MS spectra obtained for the parent compound and the proposed fragmentation pathways, respectively. Additionally, the MS/MS spectra obtained for TPs are presented in Figures S7–S9. Based on the structure of the TP, a schematic proposal of the modifications induced by the photocatalytic process on LEV is

shown in Figure 4. It should be mentioned that another abundant TP (having the empirical formula  $C_{18}H_{19}N_3O_6F$ ) was observed. However, its elucidation was not possible, and therefore, it was not included in Figure 4.

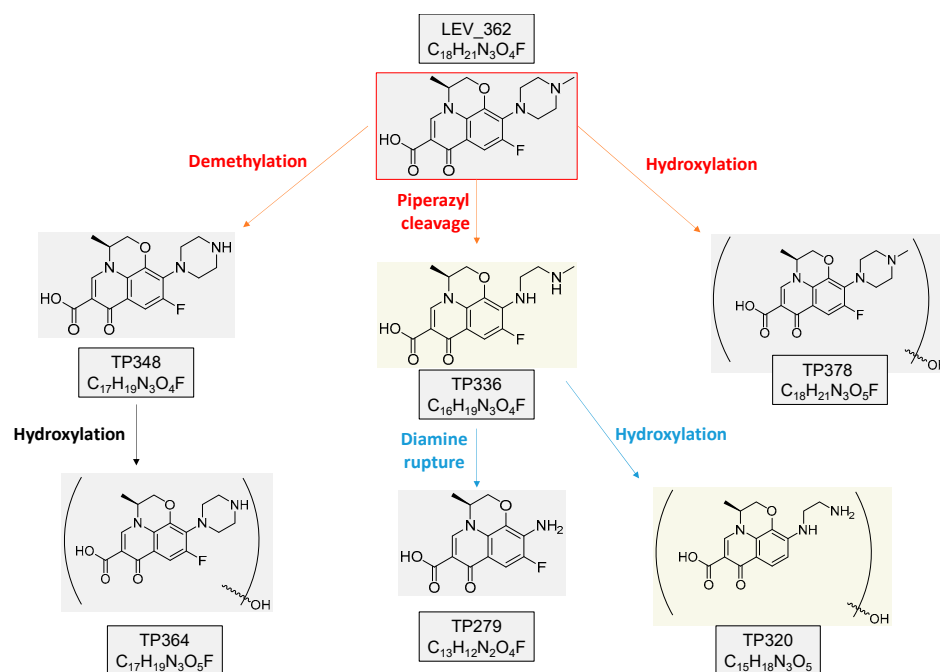


**Figure 4.** Schema of the primary transformations of LEV under photocatalysis using CdS.

### 3.5. Degradation of Levofloxacin in Complex Matrices

The degradation efficiency of the photocatalytic processes is strongly dependent on both the pH and matrix components of water [9,29]. Hence, the photocatalytic elimination of the target pollutant at diverse pH values was assessed. Furthermore, the degradation in matrices more complex than distilled water, i.e., synthetic fresh urine (urine) and simulated hospital wastewater (HWW), which are primary sources of pollution by pharmaceuticals, was considered (see matrix composition in Tables 2 and 3). Figure 5 compares the degradation rate for LEV at the tested pH values. Furthermore, the control experiments of LEV photolysis (as a function of pH) were also included in this figure.

**Table 2.** Composition of the simulated urine <sup>1</sup>.

Compound	Concentration (mM)
Urea	266.40
NaCH <sub>3</sub> COO	125.00
Na <sub>2</sub> SO <sub>4</sub>	16.19
NH <sub>4</sub> Cl	33.65
NaH <sub>2</sub> PO <sub>4</sub>	24.17
KCl	56.34
MgCl <sub>2</sub>	3.89
CaCl <sub>2</sub>	4.60
NaOH	3.00

pH: 6.1

<sup>1</sup> Composition taken from Amstutz et al. [30].



**Table 3.** Composition of the simulated hospital wastewater (HWW) <sup>1</sup>.

Compound	Concentration (mM)
Urea	20.98
Na <sub>2</sub> SO <sub>4</sub>	0.71
NH <sub>4</sub> Cl	0.93
KH <sub>2</sub> PO <sub>4</sub>	0.37
KCl	1.34
CaCl <sub>2</sub> × 2H <sub>2</sub> O	0.34
NaCl	50.05

pH: 5.3

<sup>1</sup> Composition taken from [31].

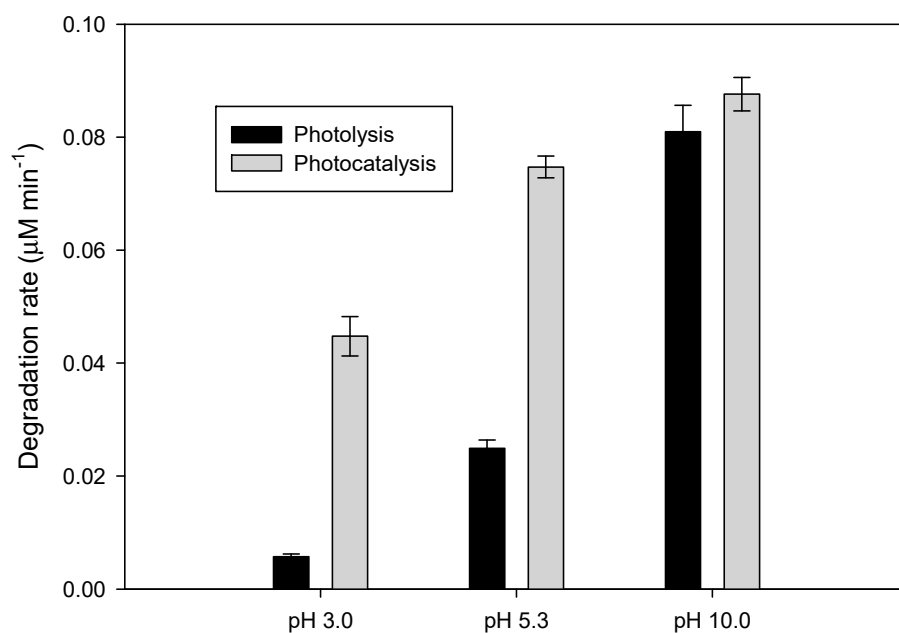


**Figure 5.** Effect of pH on the degradation of LEV by the photolytic (UVA alone) and photocatalytic (UVA/CdS) processes. Experimental conditions: [LEV] = 13.8 µM, [CdS] = 0.5 g L<sup>-1</sup>, and UVA intensity = 40 W m<sup>-2</sup>.

Regarding the LEV elimination in urine and HWW, it must be indicated that the treatments were carried out and the corresponding degradation rates in such matrices were established. Then, to analyze the selectivity of the photocatalytic process to remove LEV from urine and HWW, a ratio ( $\rho$ ) between the degradation rate in the matrix and the degradation rate in distilled water was calculated (Equation (11)). Figure 6 shows the  $\rho$ -values for the degradation of LEV in the matrices under study. A  $\rho$ -value close to 1 indicates that the process is highly selective for the elimination of LEV in the considered matrix, whereas a  $\rho$ -value close to 0 means that the process is strongly affected by the matrix components.

$$\rho = \text{rate in the matrix} / \text{rate in distilled water.} \quad (11)$$

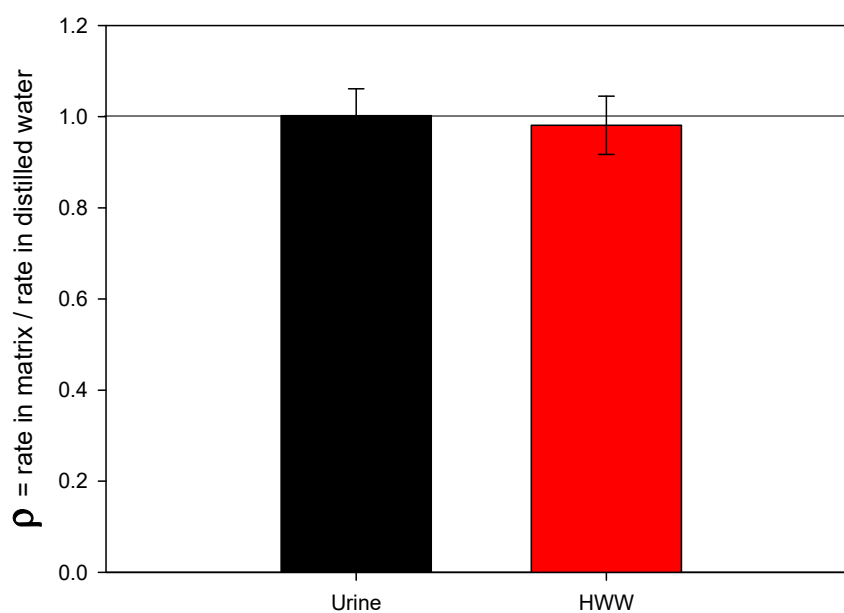


**Figure 6.** Selectivity of LEV degradation in synthetic urine and simulated hospital wastewater (HWW). Experimental conditions: [LEV] = 13.8  $\mu\text{M}$ , [CdS] = 0.5  $\text{g L}^{-1}$ , UVA intensity = 40  $\text{W m}^{-2}$ , and initial pH = 5.3.

## 4. Discussion

### 4.1. Characterization

The RAMAN spectra for the prepared CdS (Figure 1a,b) showed the typical signals for the longitudinal optical modes (LO) of CdS. The fundamental frequency at  $\sim 300 \text{ cm}^{-1}$  (1LO) and the first overtone at  $\sim 600 \text{ cm}^{-1}$  (2LO) were observed. The 2LO was much less intense (I) than 1LO, resulting in an  $I_{2\text{LO}}/I_{1\text{LO}}$  ratio  $< 1$ , which reflected the nanosize and nanostructure of the prepared CdS [32]. Moreover, it can be indicated that the deconvolution of the signal at  $\sim 300 \text{ cm}^{-1}$  (Figure 1a), revealed the presence of two peaks at 295 and 305  $\text{cm}^{-1}$ , which also confirmed that the prepared material was CdS [33].

The SEM image (Figure 1c) indicated that, in the prepared material, the surface was not homogenous, and a mixture of hexagonal crystals and distorted cubes was observed. This could be associated with a synthesis process controlled by nucleation (which can be dominated by nucleation of the ion-by-ion type). Furthermore, the microcrystalline structures had a high degree of disorder, suggesting that crystallites had many small regions of  $\alpha$ -CdS coexisting with many small regions of  $\beta$ -CdS. The TEM image of CdS (Figure 1d) showed that this material had an average diameter of 3–5 nm, consistent with the size of nanostructures for CdS reported in the literature [32,34]. The TEM image also showed that the shape of the CdS nanoparticles can be rods and spherical prolates [32], coherent with the observed in the SEM results.

From the  $\text{N}_2$  adsorption–desorption analysis (Figure 1f), an isotherm type III with an H3 hysteresis loop (i.e., particles giving rise to slit-shaped pores) was identified, according to the IUPAC classification. This is typical for materials that have a low  $S_{\text{BET}}$  and pore volume, which is the case for synthesized CdS.

The EDS result was in accordance with the expected stoichiometry, indicating that cadmium and sulfide were found at a 1:1 ratio. Additionally, the CdS presented an  $E_{\text{gap}}$  of 2.63 eV (Figure 1e), which is consistent with the value reported in the literature [35]. Moreover, the  $E_{\text{gap}}$  indicates that the catalyst can be activated with light having a wavelength lower than 470 nm. Our results suggest that the synthesis process effectively led to the desired CdS material. This synthesis method was easy to perform, and it could be utilized in other teaching-laboratory wastes when  $\text{Cd}^{2+}$  is not mixed with other heavy metal ions.

#### 4.2. Effect of the Fluoroquinolone Structure

From Figure 2, it can be noted that NOR had a higher photolysis rate than LEV. The UV-Vis spectra for LEV and NOR (Figure S3) showed that these substances have significant absorption at 365 nm (wavelength of the main emission of the used lamps), making these antibiotics susceptible to the action of UVA. It has been reported that the photochemistry of fluoroquinolones is affected by their structural factors [36]. Moreover, it is recognized that electron-withdrawing substituents bonded to aromatic systems favor pathways as photo-substitution, whereas electron-donating groups disfavor such routes [37,38]. It can be noted that LEV has an electron-donating alkoxy group bonded to the aromatic ring, whereas NOR has an ethyl substituent (Table S1). This explains the lower degradation rate of LEV by UVA irradiation (Figure 2).

As also shown in Figure 2, the presence of CdS accelerates the degradation of both pollutants. The degradation rate of NOR augmented from 0.133 to 0.155  $\mu\text{M min}^{-1}$ , whereas for LEV the rate increased from 0.0421 to 0.0818  $\mu\text{M min}^{-1}$ . Remarkably, the improvement in LEV elimination was more significant than in the NOR case. These degradations enhancement could be associated with the action of degrading species generated from the interaction of CdS with UVA irradiation (Equations (1)–(6)). Due to the lower photo-degradation of LEV, this fluoroquinolone is more susceptible to the improvement of elimination by the photocatalytic process. Furthermore, considering the more relevant role of CdS in the degradation of levofloxacin, the next steps of the work were performed using levofloxacin as the target pollutant.

#### 4.3. Effect of the Concentration of Fluoroquinolone

From Figure S4, it can be noted that the curves representing the concentration effect for the photolytic (UVA alone) and photocatalytic (UVA/CdS) systems had different shapes, which suggests different kinetics behaviors among the processes. This is logical according to the nature of the systems. The photolytic process exhibited a linear response for the degradation rate with an increasing pollutant concentration; for example, as higher amounts of LEV were in the solution, more photons of UVA can be used to transform this fluoroquinolone. Table 1 shows a  $k$ -value of  $2.0 \times 10^{-3} \text{ min}^{-1}$  for the photolytic degradation of the pollutant by UVA, which is comparable to that reported in previous works on the photodegradation of LEV ( $0.167\text{--}1.807 \times 10^{-3} \text{ min}^{-1}$ ) [39]. Additionally, the average percentage error (APE) was low (i.e., <10%), which denotes a good adjustment of experimental data to the model.

In the case of photocatalysis, an increase in the degradation rate was also observed when increasing the initial concentration of the pollutant. When the concentration of the pollutant rises, it becomes easier for the degrading species to attack LEV. However, the trend line for CdS-photocatalysis suggests that between 13.8–23.4  $\mu\text{M}$ , the system reaches a plateau (Table 1 and Figure S4). From the fitting to the L-H model, it was found that the values of  $k_{\text{L-H}}$  and  $K_{\text{L-H}}$  were small ( $0.112 \mu\text{M min}^{-1}$  and  $0.126 \mu\text{M}^{-1}$ , respectively), which indicates slow degradation kinetics and moderate adsorption affinity of the LEV toward the CdS surface. As the degradation of LEV by the CdS-photocatalytic process has not been published, there is not enough information to directly compare our results with the literature. However, it should be mentioned that the elimination of other fluoroquinolones as norfloxacin or moxifloxacin by  $\text{TiO}_2$ -photocatalysis also adjusted well to the L-H model [40,41]. It is worth noticing that the comparison of results about the degradation rate (Figure S4) evidences that the photocatalytic process had a higher rate of LEV removal than the photolytic system, indicating again the superiority of the former process at the tested concentrations.

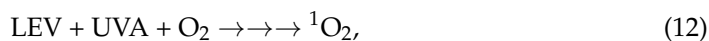
#### 4.4. Routes of Degradation and Primary Transformations of Levofloxacin

The  $R_r$  parameter for BQ, KI, and FFA had values lower than 0.5 (Figure 3), indicating that these substances strongly inhibited the LEV degradation. Meanwhile, IPA showed a value of  $R_r$  higher than 0.9, suggesting a low inhibition of LEV degradation by its presence.

These results indicate that superoxide anion radical, holes in the surface of CdS, and singlet oxygen had significant participation in the LEV degradation by CdS-photocatalysis, while hydroxyl radical in bulk had a very low contribution.

These degradation routes can be rationalized taking into account the photochemistry of both LEV and CdS. As mentioned above, the interaction of UVA light with the catalyst induces the generation of holes (Equation (1)). The redox potential of CdS holes is low ( $E^\circ \sim 1.3$  V, [42]); thus, the direct formation of  $\text{HO}^\bullet$  from water oxidation is not plausible, but some hydroxyl radicals can be generated through a reductive route involving  $\text{O}_2^{\bullet-}$  (Equations (3)–(5)). However, as superoxide anion radical reacts with LEV, the formation of  $\text{HO}^\bullet$  is low. Consequently, the  $\text{HO}^\bullet$  participation in the LEV degradation by photocatalysis with CdS was low, as indicated by Figure 3.

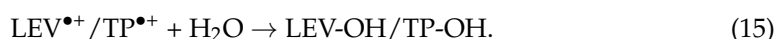
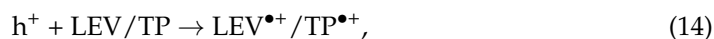
The high participation of singlet oxygen in the LEV degradation is justified, considering that such degrading species are produced from the irradiation of LEV (Equation (12)) [36,43]. Furthermore, the photo-generated holes from the CdS can interact with the superoxide anion radical to produce singlet oxygen (Equation (13)) [27]. Then, the formed singlet oxygen reacts with the LEV fluoroquinolone, leading to its degradation [43,44].



In turn, the primary transformation products (TPs) showed that the photocatalytic process induced strong LEV modifications on the methyl-piperazyl moiety, plus hydroxylation of the fluoroquinolone nucleus (Figure 4). Reactive oxygen species (ROS) such as singlet oxygen or superoxide anion radical attack the electron-rich moieties (such as the piperazyl ring) on fluoroquinolones [43]. The  ${}^1\text{O}_2$  or  $\text{O}_2^{\bullet-}$  were able to induce demethylation and cleavage of piperazyl moiety, leading to the formation of TP348, TP336, and TP279.

It has been reported that singlet oxygen and superoxide anion radical promote the demethylation of tertiary amides [45], similarly to the terminal one on the piperazyl moiety of LEV. The demethylation of amide involves an initial electron transfer from the excited fluoroquinolone to oxygen, producing the addition of oxygen with the subsequent loss of the methyl group (Figure S10), as reported for rifloxacin [45]. Moreover, superoxide anion radical induces the rupture of piperazyl moiety, which is also initiated by an electron transfer, plus the formation of a peroxy-piperazyl structure, followed by an opening of the piperazyl ring (Figure S11), analogously to that informed for ciprofloxacin (another fluoroquinolone antibiotic) during its treatment by  $\text{TiO}_2$ -photocatalysis [46] or single photolysis [36].

Unlike other semiconductors (e.g.,  $\text{TiO}_2$  or  $\text{ZnO}$ ), CdS does not produce hydroxyl radicals through photo-generated holes. However, organic compounds can directly react with  $\text{h}^+$  [47]. The holes of CdS can abstract electrons from the aromatic structure of the parent fluoroquinolone (LEV) or some primary transformation products (e.g., TP336 or TP348), generating unstable species that interact with water to form hydroxylated products [8] (Equations (14) and (15)). This last explains the formation of TP378, TP364, and TP320.



Based on the transformations induced by the photocatalytic process, the treated solutions of LEV should exhibit a lower antimicrobial activity (AA) than the initial sample. It is recognized that the cleavage of the piperazyl ring decreases the antibacterial properties of fluoroquinolones, due to this functional group controls the potency and pharmacokinetic aspects of these pharmaceuticals [48,49].

#### 4.5. Effect of the Matrix on the Degradation of Levofloxacin

Figure 5 reveals that the antibiotic degradation was faster when the pH increased. Nevertheless, as the pH was higher, the difference between LEV degradation upon photolysis and CdS-photocatalysis was lower. In fact, at the basic pH, the LEV elimination by both systems had the same rate. In contrast, it has been reported that CdS has a point of zero charge (PZC), being  $\sim 5.7$ . Then, at a lower pH than the PZC, the catalyst surface is positively charged, while at a higher pH than the PZC, CdS is negatively charged [34,50]. LEV is cationic below its  $pK_{a1}$  (which is 5.59), anionic above its  $pK_{a2}$  (which is 7.94), and a zwitterion between  $pK_{a1}$  and  $pK_{a2}$ . Thus, the effect of pH on the elimination of LEV cannot be solely rationalized in terms of the ionization state of the pharmaceutical and CdS. Due to both the pharmaceutical and CdS being positive or negative in acidic or basic environments, the adsorption of the pollutant onto the surface of the catalyst is disfavored. Hence, the photolytic route could play a relevant role in this case.

It can be mentioned that an increase in the photolysis of LEV as the pH rises could be associated with the acid-base speciation of the pollutant. As the pH of the solution increases, functional groups such as carboxylic acid and piperazyl of the antibiotic lose their hydrogens (see Figure S12). At pH 3.0, both  $-\text{COOH}$  and  $=\text{N}(\text{CH}_3)\text{H}^+$  on LEV are protonated, at pH 5.3 the secondary amine of piperazyl retains the hydrogen, and at pH 10 both carboxylic acid and amine were deprotonated (i.e., LEV has  $-\text{COO}^-$  and  $=\text{N}(\text{CH}_3)$  moieties). When the levofloxacin releases such hydrogens, it gains electron density. Therefore, there is a higher electron availability on the LEV structure, which makes more feasible the excitation by light action (i.e., photolytic processes can be favored). In fact, it is already reported that the dissociation of the carboxylic acid group on LEV enhances the rate of degradation, and similarly, the deprotonation of the piperazyl group also improves the rate of degradation [39]. These aspects explain the predominance of the photolytic route at pH 10. Nevertheless, it should be noted that at pH values of 3.0 and 5.3, there were significant differences between the photolytic and photocatalytic systems (Figure 5). At these two pH conditions, the reactive oxygen species (such as singlet oxygen and superoxide anion radical resulting from the CdS action; Equations (1)–(6)) had strong participation in LEV degradation because of the low contribution of the photolytic route (Figure 5). As mentioned above, LEV has a higher electron availability to be attacked by  $^1\text{O}_2$  and  $\text{O}_2^{\bullet-}$ . Singlet oxygen is an electrophilic species that present a higher reactivity toward electron-rich moieties on organic pollutants [51]. In turn, superoxide anion radical can attack double bonds [52,53]. Moreover, a recent work has shown that moieties as piperazyl on LEV are very prone to attacks by electrophiles [31].

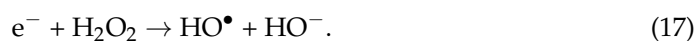
Regarding pharmaceutical elimination in complex matrices (Figure 6), it can be noted that the photocatalytic process using CdS is highly selective for the degradation of LEV in the urine and HWW, as indicated by the  $\rho$ -values very close to 1. These results can be understood by considering the degrading agents involved in the process. As shown above, both singlet oxygen and superoxide anion radical are the main factors responsible for LEV elimination, and for pollutants that have high reactivity with such species, the organic (e.g., urea and acetate) and inorganic (e.g., chloride, sulfate, and dihydrogen phosphate) components of the matrix exhibit little interference [51,53,54]. This contrasts with the typical competition of matrix components in other photocatalytic processes. For instance, the degradation of pharmaceuticals in urine by  $\text{TiO}_2$ -photocatalysis (which involves the action of  $\text{HO}^\bullet$  and  $\text{h}^+$ ) is affected by the urine matrix [55].

On the contrary, we should mention that after the use of the catalyst, the quantification of dissolved cadmium revealed  $\sim 49 \text{ mg L}^{-1}$  of  $\text{Cd}^{2+}$  in the solution. This drawback of the photocatalytic process using CdS is associated with the catalyst photo-corrosion in aqueous media [42]. The hole ( $\text{h}^+$ ) oxidizes the solid, releasing  $\text{Cd}^{2+}$  (Equation (16)) [7]. To deal with this disadvantage, the synthesis method described in Section 2 could be applied to recover the CdS after the pollutant treatment. Another alternative may be the utilization of CdS in the presence of sulfur-containing organic compounds (e.g., thiourea) to limit photo-corrosion [7]. Despite the drawback of the photo-corrosion of CdS, the process

demonstrated good results for the elimination of fluoroquinolones in complex matrices (as shown in Figure 6). Additionally, the use of CdS-photocatalysis in small volumes (a few liters) makes the recovery of the released  $\text{Cd}^{2+}$  easier than at a large scale. Thus, this photocatalytic process could be tested in point-of-use systems to treat urine (with a median value of 1.4 L/person/day [56]) containing pharmaceuticals.



Finally, we can remark that all of the above results support the proof of concept for the preparation of catalysts from laboratory wastes and their subsequent use to degrade organic pollutants in aqueous matrices (e.g., fresh urine), and also contribute to the understanding of the fundamental aspects (such as degradation routes, primary transformations, and matrix and concentration effects) involved in the photocatalytic process. However, it is very important to mention that in the particular case of CdS-photocatalysis, for those pollutants with low reactivity toward singlet oxygen, and superoxide radical anion, this process would have low action because of the inefficient production of hydroxyl radicals directly, which limits the practical applications of the process. Thus, in future research, the addition of hydrogen peroxide (which can react with the electrons in the conduction band; Equation (17)), or the heterojunction with other materials (e.g.,  $\text{SnO}_2$ ) could provide interesting options to increase the generation of  $\text{HO}^\bullet$  [57], to favor the degradation of pollutants with low reactivity toward  $^1\text{O}_2$  or  $\text{O}_2^{\bullet-}$ .



**Supplementary Materials:** The following are available online at <https://www.mdpi.com/article/10.3390/w13162154/s1>, Figure S1: Reaction system, Figure S2: Initial rate of degradation ( $r$ ) determination, Figure S3: UV-Vis Spectra of NOR (a) and LEV (b), Figure S4: Effect of the pollutant concentration on the degradation of LEV by photolysis (UVA alone) and photocatalysis (UVA/CdS), Figure S5: MS/MS spectra for levofloxacin at different collision energies (from bottom to top: 10, 20, 30, 40, and 50 eV), Figure S6: Fragmentation pathway proposed for levofloxacin, Figure S7: MS/MS spectra obtained for TP279 at different collision energies (from bottom to top: 10, 20, 30, 40, and 50 eV), Figure S8: MS/MS spectra obtained for TP364 at different collision energies (from bottom to top: 10, 20, 30, 40, and 50 eV), Figure S9: MS/MS spectra obtained for TP336 at different collision energies (from bottom to top: 10, 20, 30, 40, and 50 eV), Figure S10: Demethylation of LEV by singlet oxygen or superoxide anion radical, Figure S11: Piperazyl breakdown promoted by superoxide anion radical, Figure S12: Deprotonation of LEV as the pH increases, Table S1: Chemical structures of NOR and LEV.

**Author Contributions:** Conceptualization, R.A.T.-P., Y.Á.-T. and E.A.S.-G.; methodology, E.A.S.-G. and M.I.; elucidation of transformation products by HRMS, M.I. and F.H.; formal analysis, Y.Á.-T. and E.A.S.-G.; investigation, Y.Á.-T. and E.A.S.-G.; writing—original draft preparation, E.A.S.-G.; writing—review and editing, R.A.T.-P., Y.Á.-T., M.I. and F.H.; project administration, Y.Á.-T.; funding acquisition, R.A.T.-P. and Y.Á.-T. All authors have read and agreed to the published version of the manuscript.

**Funding:** This research was funded by UNIVERSIDAD SANTIAGO DE CALI, grant number DGI 939-621120-1867, and UNIREMINGTON, grant number 400000287 (contract No. 80740-680-2020). The authors from UJI acknowledge the financial support from the Ministry of Science Innovation and University, Spain (Ref. RTI2018-097417-B-I00) to develop their research on emerging contaminants, as well as the Generalitat Valenciana (Research Group of Excellence, Prometeo 2019/040). Efraim Serna-Galvis thanks MINCIENCIAS COLOMBIA for his postdoctoral fellowship, Convocatoria 848 de 2019. The APC was funded by UNIVERSIDAD SANTIAGO DE CALI.

**Institutional Review Board Statement:** Not applicable.

**Informed Consent Statement:** Not applicable.

**Data Availability Statement:** Data is contained within the article or Supplementary Materials.



**Acknowledgments:** The authors thank Melissa Suárez-Jiménez, Brandon Suárez-Jiménez, and Angie Lasso-Escobar their help in the preparation of some of the experimental tests. Moreover, Efraim Serna-Galvis thanks Jazmin Porras for her technical support in finishing the present research.

**Conflicts of Interest:** The authors declare no conflict of interest.

## References

1. Velenturf, A.P.M.; Purnell, P. Principles for a sustainable circular economy. *Sustain. Prod. Consum.* **2021**, *27*, 1437–1457. [CrossRef]
2. Nascimento, E.D.S.; Filho, A.T. Chemical waste risk reduction and environmental impact generated by laboratory activities in research and teaching institutions. *Braz. J. Pharm. Sci.* **2010**, *46*, 187–198. [CrossRef]
3. Allen, R.O. Waste disposal in the laboratory: Teaching responsibility and safety. *J. Chem. Educ.* **1983**, *60*, A81. [CrossRef]
4. Green Facts. Cadmium. Available online: <https://www.greenfacts.org/en/cadmium/index.htm#:~:text=It%20mainly%20affects%20kidneys%20and,%2C%20animals%20and%20micro-organisms> (accessed on 1 June 2020).
5. Minnesota Department of Health. *Cadmium and Drinking Water*; Minnesota Department of Health: St. Paul, MN, USA, 2014. Available online: <https://www.health.state.mn.us/communities/environment/risk/docs/guidance/gw/cadmiuminfo.pdf> (accessed on 25 June 2021).
6. Cheng, L.; Xiang, Q.; Liao, Y.; Zhang, H. CdS-Based photocatalysts. *Energy Environ. Sci.* **2018**, *11*, 1362–1391. [CrossRef]
7. Davis, A.P.; Huang, C.P. The photocatalytic oxidation of sulfur-containing organic compounds using cadmium sulfide and the effect on CdS photocorrosion. *Water Res.* **1991**, *25*, 1273–1278. [CrossRef]
8. Davis, A.P.; Huang, C.P. The removal of substituted phenols by a photocatalytic oxidation process with cadmium sulfide. *Water Res.* **1990**, *24*, 543–550. [CrossRef]
9. Villegas-Guzman, P.; Silva-Agredo, J.; González-Gómez, D.; Giraldo-Aguirre, A.L.; Flórez-Acosta, O.; Torres-Palma, R.A. Evaluation of water matrix effects, experimental parameters, and the degradation pathway during the TiO<sub>2</sub> photocatalytic treatment of the antibiotic dicloxacillin. *J. Environ. Sci. Health Part A* **2015**, *50*, 40–48. [CrossRef] [PubMed]
10. Granda-Ramírez, C.F.; Hincapié-Mejía, G.M.; Serna-Galvis, E.A.; Torres-Palma, R.A. Degradation of Recalcitrant Safranin T Through an Electrochemical Process and Three Photochemical Advanced Oxidation Technologies. *Water Air Soil Pollut.* **2017**, *228*, 1–12. [CrossRef]
11. Serna-Galvis, E.A.; Giraldo-Aguirre, A.L.; Silva-Agredo, J.; Florez-Acosta, O.A.; Torres-Palma, R.A. Removal of antibiotic cloxacillin by means of electrochemical oxidation, TiO<sub>2</sub> photocatalysis, and photo-Fenton processes: Analysis of degradation pathways and effect of the water matrix on the elimination of antimicrobial activity. *Environ. Sci. Pollut. Res.* **2017**, *24*, 6339–6352. [CrossRef]
12. Serna-Galvis, E.A.; Silva-Agredo, J.; Giraldo, A.L.; Flórez, O.A.; Torres-Palma, R.A. Comparison of route, mechanism and extent of treatment for the degradation of a  $\beta$ -lactam antibiotic by TiO<sub>2</sub> photocatalysis, sonochemistry, electrochemistry and the photo-Fenton system. *Chem. Eng. J.* **2016**, *284*, 953–962. [CrossRef]
13. Bahnemann, D. Photocatalytic formation of sulfur-centered radicals by one-electron redox processes on semiconductor surfaces. In *Sulfur-Centered Reactive Intermediates in Chemistry and Biology*; Chatgililoglu, C., Asmus, K.-D., Eds.; Springer: Boston, MA, USA, 1990; pp. 103–120, ISBN 978-1-4684-5876-3.
14. Armstrong, D.A.; Huie, R.E.; Lyman, S.; Koppenol, W.H.; Merényi, G.; Neta, P.; Stanbury, D.M.; Steenken, S.; Wardman, P. Standard electrode potentials involving radicals in aqueous solution: Inorganic radicals. *Bioinorg. React. Mech.* **2013**, *9*, 59–61. [CrossRef]
15. IUPAC Task Group on Radical Electrode Potentials. *Standard Electrode Potentials Involving Radicals in Aqueous Solution: Inorganic Radicals*; IUPAC: Research Triangle Park, NC, USA, 2016.
16. Bijlsma, L.; Pitarch, E.; Fonseca, E.; Ibáñez, M.; Botero, A.M.; Claros, J.; Pastor, L.; Hernández, F. Investigation of pharmaceuticals in a conventional wastewater treatment plant: Removal efficiency, seasonal variation and impact of a nearby hospital. *J. Environ. Chem. Eng.* **2021**, *9*, 105548. [CrossRef]
17. Van Doorslaer, X.; Dewulf, J.; Van Langenhove, H.; Demeestere, K. Fluoroquinolone antibiotics: An emerging class of environmental micropollutants. *Sci. Total Environ.* **2014**, *500–501*, 250–269. [CrossRef] [PubMed]
18. Speltini, A.; Sturini, M.; Maraschi, F.; Profumo, A. Fluoroquinolone antibiotics in environmental waters: Sample preparation and determination. *J. Sep. Sci.* **2010**, *33*, 1115–1131. [CrossRef] [PubMed]
19. Botero-Coy, A.M.; Martínez-Pachón, D.; Boix, C.; Rincón, R.J.; Castillo, N.; Arias-Marín, L.P.; Manrique-Losada, L.; Torres-Palma, R.A.; Moncayo-Lasso, A.; Hernández, F. An investigation into the occurrence and removal of pharmaceuticals in Colombian wastewater. *Sci. Total Environ.* **2018**, *642*, 842–853. [CrossRef] [PubMed]
20. Drlica, K.; Zhao, X.; Malik, M.; Hiasa, H.; Mustaev, A.; Kerns, R. Fluoroquinolone resistance. *Bact. Resist. Antibiot. Mol. Man* **2019**, *317*, 125–161. [CrossRef]
21. López, R.; Gómez, R. Band-gap energy estimation from diffuse reflectance measurements on sol-gel and commercial TiO<sub>2</sub>: A comparative study. *J. Sol-Gel Sci. Technol.* **2012**, *61*, 1–7. [CrossRef]
22. Serna-Galvis, E.A.; Isaza-Pineda, L.; Moncayo-Lasso, A.; Hernández, F.; Ibáñez, M.; Torres-Palma, R.A. Comparative degradation of two highly consumed antihypertensives in water by sonochemical process. Determination of the reaction zone, primary degradation products and theoretical calculations on the oxidative process. *Ultrason. Sonochem.* **2019**, *58*, 104635. [CrossRef]

23. Fang, Z.; Guo, T.; Welz, B. Determination of cadmium, lead and copper in water samples by flame atomic-absorption spectrometry with preconcentration by flow-injection on-line sorbent extraction. *Talanta* **1991**, *38*, 613–619. [[CrossRef](#)]
24. Kumar, K.V.; Porkodi, K.; Rocha, F. Langmuir–Hinshelwood kinetics—A theoretical study. *Catal. Commun.* **2008**, *9*, 82–84. [[CrossRef](#)]
25. Chiha, M.; Merouani, S.; Hamdaoui, O.; Baup, S.; Gondrexon, N.; Pétrier, C. Modeling of ultrasonic degradation of non-volatile organic compounds by Langmuir-type kinetics. *Ultrason. Sonochem.* **2010**, *17*, 773–782. [[CrossRef](#)]
26. Kaur, A.; Umar, A.; Anderson, W.A.; Kansal, S.K. Facile synthesis of CdS/TiO<sub>2</sub> nanocomposite and their catalytic activity for ofloxacin degradation under visible illumination. *J. Photochem. Photobiol. A Chem.* **2018**, *360*, 34–43. [[CrossRef](#)]
27. Wang, F.; Feng, Y.; Chen, P.; Wang, Y.; Su, Y.; Zhang, Q.; Zeng, Y.; Xie, Z.; Liu, H.; Liu, Y.; et al. Photocatalytic degradation of fluoroquinolone antibiotics using ordered mesoporous g-C<sub>3</sub>N<sub>4</sub> under simulated sunlight irradiation: Kinetics, mechanism, and antibacterial activity elimination. *Appl. Catal. B Environ.* **2018**, *227*, 114–122. [[CrossRef](#)]
28. Palominos, R.; Freer, J.; Mondaca, M.A.; Mansilla, H.D. Evidence for hole participation during the photocatalytic oxidation of the antibiotic flumequine. *J. Photochem. Photobiol. A Chem.* **2008**, *193*, 139–145. [[CrossRef](#)]
29. Villegas-Guzman, P.; Silva-Agredo, J.; Florez, O.; Giraldo-Aguirre, A.L.; Pulgarin, C.; Torres-Palma, R.A. Selecting the best AOP for isoxazolyl penicillins degradation as a function of water characteristics: Effects of pH, chemical nature of additives and pollutant concentration. *J. Environ. Manag.* **2017**, *190*, 72–79. [[CrossRef](#)]
30. Amstutz, V.; Katsaounis, A.; Kapalka, A.; Comminellis, C.; Udert, K.M. Effects of carbonate on the electrolytic removal of ammonia and urea from urine with thermally prepared IrO<sub>2</sub> electrodes. *J. Appl. Electrochem.* **2012**, *42*, 787–795. [[CrossRef](#)]
31. Serna-Galvis, E.A.; Jojoa-Sierra, S.D.; Berrio-Perlaza, K.E.; Ferraro, F.; Torres-Palma, R.A. Structure-reactivity relationship in the degradation of three representative fluoroquinolone antibiotics in water by electrogenerated active chlorine. *Chem. Eng. J.* **2017**, *315*, 552–561. [[CrossRef](#)]
32. Zeiri, L.; Patla, I.; Acharya, S.; Golan, Y.; Efrima, S. Raman Spectroscopy of Ultranarrow CdS Nanostructures. *J. Phys. Chem. C* **2007**, *111*, 11843–11848. [[CrossRef](#)]
33. Nanda, K.K.; Sarangi, S.N.; Sahu, S.N.; Deb, S.K.; Behera, S.N. Raman spectroscopy of CdS nanocrystalline semiconductors. *Phys. B Condens. Matter* **1999**, *262*, 31–39. [[CrossRef](#)]
34. Ludolph, B.; Malik, M.A.; O'Brien, P.; Revaprasadu, N. Novel single molecule precursor routes for the direct synthesis of highly monodispersed quantum dots of cadmium or zinc sulfide or selenide. *Chem. Commun.* **1998**, *3*, 1849–1850. [[CrossRef](#)]
35. Elsevier Semiconductors for Photocatalysis. Available online: <https://www.sciencedirect.com/topics/chemistry/cadmium-sulfide> (accessed on 3 July 2021).
36. Albini, A.; Monti, S. Photophysics and photochemistry of fluoroquinolones. *Chem. Soc. Rev.* **2003**, *32*, 238. [[CrossRef](#)] [[PubMed](#)]
37. Cornelisse, J.; Havinga, E. Photosubstitution reactions of aromatic compounds. *Chem. Rev.* **1975**, *75*, 353–388. [[CrossRef](#)]
38. Sturini, M.; Speltini, A.; Maraschi, F.; Pretali, L.; Profumo, A.; Fasani, E.; Albini, A.; Migliavacca, R.; Nucleo, E. Photodegradation of fluoroquinolones in surface water and antimicrobial activity of the photoproducts. *Water Res.* **2012**, *46*, 5575–5582. [[CrossRef](#)]
39. Ahmad, I.; Bano, R.; Sheraz, M.A.; Ahmed, S.; Mirza, T.; Ansari, S.A. Photodegradation of levofloxacin in aqueous and organic solvents: A kinetic study. *Acta Pharm.* **2013**, *63*, 223–229. [[CrossRef](#)] [[PubMed](#)]
40. Chen, M.; Chu, W. Degradation of antibiotic norfloxacin in aqueous solution by visible-light-mediated C-TiO<sub>2</sub> photocatalysis. *J. Hazard. Mater.* **2012**, *219–220*, 183–189. [[CrossRef](#)]
41. Van Doorslaer, X.; Heynderickx, P.M.; Demeestere, K.; Debevere, K.; Van Langenhove, H.; Dewulf, J. TiO<sub>2</sub> mediated heterogeneous photocatalytic degradation of moxifloxacin: Operational variables and scavenger study. *Appl. Catal. B Environ.* **2012**, *111–112*, 150–156. [[CrossRef](#)]
42. Ola, O.; Maroto-Valer, M.M. Review of material design and reactor engineering on TiO<sub>2</sub> photocatalysis for CO<sub>2</sub> reduction. *J. Photochem. Photobiol. C Photochem. Rev.* **2015**, *24*, 16–42. [[CrossRef](#)]
43. Serna-Galvis, E.A.; Ferraro, F.; Silva-Agredo, J.; Torres-Palma, R.A. Degradation of highly consumed fluoroquinolones, penicillins and cephalosporins in distilled water and simulated hospital wastewater by UV254 and UV254/persulfate processes. *Water Res.* **2017**, *122*, 128–138. [[CrossRef](#)]
44. Niu, X.-Z.; Busetti, F.; Langsa, M.; Croué, J.-P. Roles of singlet oxygen and dissolved organic matter in self-sensitized photo-oxidation of antibiotic norfloxacin under sunlight irradiation. *Water Res.* **2016**, *106*, 214–222. [[CrossRef](#)]
45. Belvedere, A.; Boscá, F.; Cuquerella, M.C.; de Guidi, G.; Miranda, M.A. Photoinduced N-Demethylation of Rufloxacin and its Methyl Ester Under Aerobic Conditions. *Photochem. Photobiol.* **2002**, *76*, 252. [[CrossRef](#)]
46. Salma, A.; Thorøe-Boveleth, S.; Schmidt, T.C.; Tuerk, J. Dependence of transformation product formation on pH during photolytic and photocatalytic degradation of ciprofloxacin. *J. Hazard. Mater.* **2016**, *313*, 49–59. [[CrossRef](#)]
47. Davis, A.P.; Huang, C.P. Water treatment and quality alteration. In *Selected Water Resources Abstracts*; NTIS, Ed.; Geological Survey U.S., Department of Interior: Washington, DC, USA, 1990.
48. Peterson, L.R. Quinolone molecular structure-activity relationships: What we have learned about improving antimicrobial activity. *Clin. Infect. Dis.* **2001**, *33*, S180–S186. [[CrossRef](#)]
49. Aldred, K.J.; Kerns, R.J.; Osheroff, N. Mechanism of quinolone action and resistance. *Biochemistry* **2014**, *53*, 1565–1574. [[CrossRef](#)] [[PubMed](#)]
50. Kaur, M.; Mehta, S.K.; Kansal, S.K. Visible light driven photocatalytic degradation of ofloxacin and malachite green dye using cadmium sulphide nanoparticles. *J. Environ. Chem. Eng.* **2018**, *6*, 3631–3639. [[CrossRef](#)]

51. Díez-Mato, E.; Cortezón-Tamarit, F.C.; Bogialli, S.; García-Fresnadillo, D.; Marazuela, M.D. Phototransformation of model micropollutants in water samples by photocatalytic singlet oxygen production in heterogeneous medium. *Appl. Catal. B Environ.* **2014**, *160–161*, 445–455. [[CrossRef](#)]
52. Danen, W.C.; Warner, R.J.; Arudi, R.L. Nucleophilic Reactions of Superoxide Anion Radical. In *Organic Free Radicals*; ACS Symposium Series; American Chemical Society: Washington, DC, USA, 1978; Volume 69, pp. 244–257.
53. Hayyan, M.; Hashim, M.A.; Alnashef, I.M. Superoxide Ion: Generation and Chemical Implications. *Chem. Rev.* **2016**, *116*, 3029–3085. [[CrossRef](#)] [[PubMed](#)]
54. Liu, T.; Zhang, D.; Yin, K.; Yang, C.; Luo, S.; Crittenden, J.C. Degradation of thiacloprid via unactivated peroxymonosulfate: The overlooked singlet oxygen oxidation. *Chem. Eng. J.* **2020**, *388*, 124264. [[CrossRef](#)]
55. Guateque-Londoño, J.F.; Serna-Galvis, E.A.; Silva-Agredo, J.; Ávila-Torres, Y.; Torres-Palma, R.A. Dataset on the degradation of losartan by TiO<sub>2</sub>-photocatalysis and UVC/persulfate processes. *Data Brief* **2020**, *31*, 105692. [[CrossRef](#)]
56. Rose, C.; Parker, A.; Jefferson, B.; Cartmell, E. The characterization of feces and urine: A review of the literature to inform advanced treatment technology. *Crit. Rev. Environ. Sci. Technol.* **2015**, *45*, 1827–1879. [[CrossRef](#)]
57. Sharma, S.; Dutta, V.; Raizada, P.; Hosseini-Bandegharai, A.; Singh, P.; Nguyen, V.H. Tailoring cadmium sulfide-based photocatalytic nanomaterials for water decontamination: A review. *Environ. Chem. Lett.* **2021**, *19*, 271–306. [[CrossRef](#)]